

Spin-modulated quasi-1D antiferromagnet LiCuVO₄

N. Büttgen* and H.-A. Krug von Nidda

*Center for Electronic Correlations and Magnetism EKM,
Experimentalphysik V, Universität Augsburg, D-86135 Augsburg, Germany*

L.E. Svistov and L.A. Prozorova

P.L.Kapitza Institute for Physical Problems RAS, 119334 Moscow, Russia

A. Prokofiev† and W. Aßmus

Physikalisches Institut, Johann-Wolfgang-Goethe-Universität, D-60054 Frankfurt, Germany

(Dated: November 12, 2018)

We report on magnetic resonance studies within the magnetically ordered phase of the quasi-1D antiferromagnet LiCuVO₄. Our studies reveal a spin reorientational transition at a magnetic field $H_{c1} \approx 25$ kOe applied within the crystallographical **ab**-plane in addition to the recently observed one at $H_{c2} \approx 75$ kOe [M.G. Banks et al., cond-mat/0608554 (2006)]. Spectra of the antiferromagnetic resonance (AFMR) along low-frequency branches can be described in the frame of a macroscopic theory of exchange-rigid planar magnetic structures. These data allow to obtain the anisotropy of the exchange interaction together with a constant of the uniaxial anisotropy. Spectra of ⁷Li nuclear magnetic resonance (NMR) show that, within the magnetically ordered phase of LiCuVO₄ in the low-field range $H < H_{c1}$, a planar spiral spin structure is realized with the spins lying in the **ab**-plane in agreement with neutron scattering studies of B.J. Gibson *et al.* [Physica B **350**, 253 (2004)]. Based on NMR spectra simulations, the transition at H_{c1} can well be described as a spin-flop transition, where the spin plane of the magnetically ordered structure rotates to be perpendicular to the direction of the applied magnetic field. For $H > H_{c2} \approx 75$ kOe, our NMR spectra simulations show that the magnetically ordered structure exhibits a modulation of the spin projections along the direction of the applied magnetic field H .

PACS numbers: 75.50.Ee, 76.60.-k, 76.50.+g, 75.10.Pq

I. INTRODUCTION

The quasi-one dimensionality (1D) of the spin system in LiCuVO₄ is provided by the magnetic ions of Cu²⁺ ($3d^9$ configuration, $S=1/2$). Lithium and copper ions share the octahedral sites in the orthorhombically distorted spinel structure in that way that the copper ions are arranged along chains separated by the non-magnetic ions of lithium, vanadium and oxygen. The temperature dependence of the magnetic susceptibility exhibits a broad maximum at around $T=28$ K, typical for low-dimensional antiferromagnets, and a sharp anomaly at $T=2.3$ K, which is associated with the establishing of three dimensional (3D) magnetic order. From the values of these temperatures, the authors of Ref. 1 evaluated the intrachain and interchain exchange integrals of 22.5 K and 1 K, respectively. Elastic neutron diffraction experiments² on single crystals of LiCuVO₄ revealed that the 3D ordered phase exhibits an incommensurate, noncollinear magnetic structure. The scheme of this magnetic structure suggested is shown in figure 1. According to that work,² the wave vector of this magnetic structure is directed along the copper chains ($\mathbf{k}_{ic} \parallel \mathbf{b}$) and the value of the ordered magnetic moments of the Cu²⁺ ions amounts to $0.31\mu_B$, lying within the **ab**-planes. The investigation of magnetic excitations in LiCuVO₄, using inelastic neutron diffraction experiments,³ confirmed the quasi-1D nature of this com-

pound and brought to conclusion that the magnetic incommensurate structure is due to an exotic ratio of intrachain exchange integrals: the nearest-neighbor exchange integral ($J_1=-18$ K) is ferromagnetic and it is strongly dominated by the value of the next-nearest exchange integral which is antiferromagnetic ($J_2=49$ K, cf. Fig. 1). This unusual hierarchy of exchange integrals is realized in LiCuVO₄ due to indirect exchange interaction through the oxygen neighborhood and it can be explained from the Goodenough-Kanamori-Anderson rules.⁴ Results of electron-band structure calculations give the values of the exchange integrals J_1 and J_2 in a good agreement with the values obtained experimentally.³ The magnetic properties of such exchange-bonded chains of Heisenberg spins with two exchange integrals J_1 and J_2 are similar to the so called "zigzag" model where pairs of chains, with an intrachain exchange integral J_1 , are coupled via an interchain exchange integral J_2 . Such model was studied theoretically in the limit of large spin values, as well as for $S=1/2$ in references 5 and 6. In these works it was shown that such a ratio of the exchange integrals, which are obtained for LiCuVO₄, results in an incommensurate magnetic structure. The value of the incommensurate vector \mathbf{k}_{ic} experimentally obtained² is found to be between theoretical values in the limit of large spin and for $S = 1/2$ (cf. Ref. 6).

Thus, LiCuVO₄ presents an example of a quasi-1D frustrated antiferromagnet of spins $S=1/2$ where strong exchange interactions yield an incommensurate non-

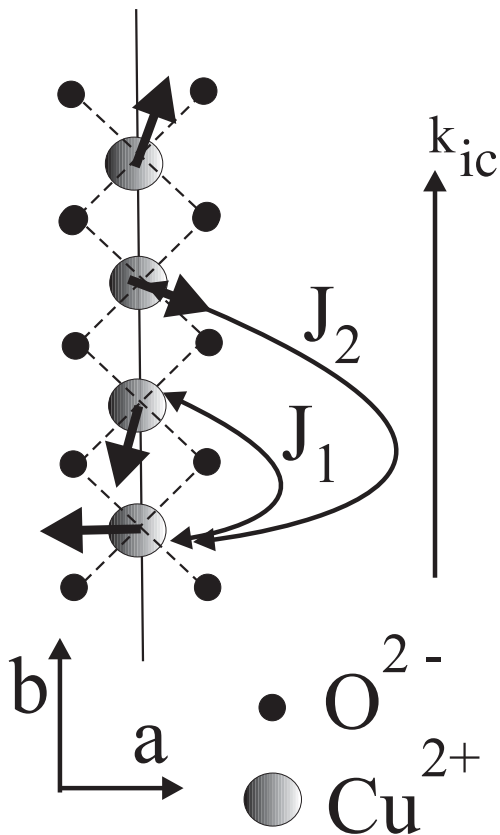


FIG. 1: Scheme of the spiral magnetic structure of LiCuVO_4 (Ref. 2). A fragment of one single chain of edge-sharing CuO_4 units along with the dominant intrachain exchange integrals J_1 and J_2 is shown.

collinear magnetically ordered structure for temperatures $T < 2.3$ K. In the present work, antiferromagnetic resonance (AFMR) and nuclear magnetic resonance (NMR) on the nuclei of nonmagnetic ions (^7Li and ^{51}V) were studied for temperatures within this magnetically ordered phase. Additionally, the AFMR experiment is extended towards elevated temperatures $T < 30$ K where 3D order already is absent, but spin correlations along copper chains are well developed. These temperatures are within the range between the maxima of the temperature dependent magnetic susceptibility $\chi(T)$ (cf. Fig. 4).

II. SAMPLE PREPARATION AND EXPERIMENTAL DETAILS

LiCuVO_4 crystallizes in an inverse spinel structure AB_2O_4 with an orthorhombic distortion stipulated by a cooperative Jahn–Teller effect, induced by Cu^{2+} ions. The crystal structure of LiCuVO_4 is described by space group Imma (Refs. 7,8). In Fig. 2, a schema of the crystal structure of LiCuVO_4 is shown. The Cu^{2+} ions, which compose strongly exchange interacting magnetic chains,

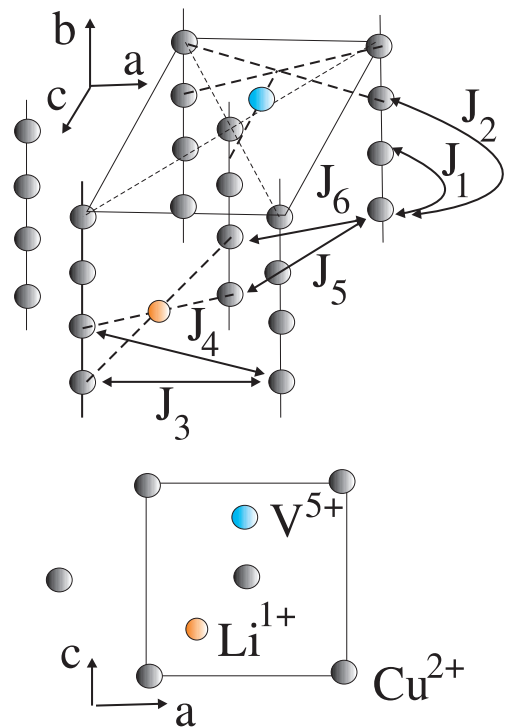


FIG. 2: Schema of the Cu^{2+} sites in the crystal structure of LiCuVO_4 . The sites of Cu^{2+} ions are marked by grey circles. One of the lithium ions is marked by an orange circle and one of the vanadium ions by a blue circle, respectively. Upper panel: J_1, \dots, J_6 denote the main exchange integrals defining the magnetic structure of LiCuVO_4 (Ref. 3). Lower panel: projection of the crystallographic structure on the ac -plane.

are marked with grey circles. For clearness these copper chains along the crystallographic \mathbf{b} -direction are joined with a solid line to guide the eye. Li^{1+} ions occupy octahedrally coordinated crystallographic equivalent sites and one of the lithium ions is marked by an orange circle. V^{5+} ions occupy the tetrahedrally coordinated crystallographic equivalent sites and one of the vanadium ions is denoted by a blue circle. The lattice parameters in \mathbf{a} - and \mathbf{c} -directions coincide with the distance between nearest copper neighbors, but along the \mathbf{b} -direction the lattice parameter equals twice the distance between nearest copper neighbors.

Single crystals with the volume of some cubic millimeters were grown as described in detail in reference 7. As the ionic radii of lithium and copper are very similar, it required special efforts to satisfy the stoichiometry of this substance. Besides of chemical methods described in Ref. 9, lithium unsoundness was controlled additionally with the NMR study of ^7Li nuclei. Detailed NMR experiments in single crystalline LiCuVO_4 in the paramagnetic phase are presented in reference 10. Figure 3 shows the NMR spectra obtained from two single crystals with different quality which are denoted (I) and (II). The spectrum of the single crystal (II) consists of several lines which

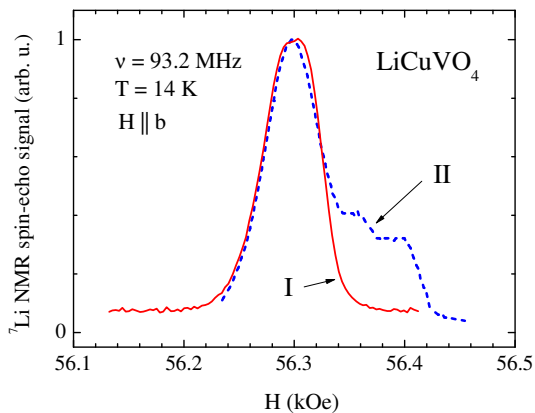


FIG. 3: ${}^7\text{Li}$ NMR spectra of single crystals from two different batches. All experiments of this work are performed with the single crystal (I).

are due to defects as it is described in reference 10. In the present work, all experiments are performed with the single crystal (I) which exhibits a single ${}^7\text{Li}$ spectral line, demonstrating a unique lithium site. This single crystal (I) was selected from the same batch as the single crystals used in references 2 and 3. The magnetic susceptibility was measured in the temperature range $1.7 < T < 400$ K with a SQUID-magnetometer MPMS7 of Quantum Design. The AFMR experiments were performed with a transmission-type spectrometer using resonators in the frequency range $18 < \nu < 110$ GHz. At elevated frequencies $65 < \nu < 250$ GHz, we employed the wave-guide-line technique. The magnetic field of a superconducting solenoid was varied in the range $0 < H < 90$ kOe. Temperatures were varied within the range $1.2 < T < 30$ K. The NMR experiments were performed with a phase coherent, homemade spectrometer at radio frequencies within the range $14.5 < \nu < 170$ MHz. We investigated the ${}^7\text{Li}$ ($I=3/2$, $\gamma/2\pi=16.5466$ MHz/T) and ${}^{51}\text{V}$ ($I=7/2$, $\gamma/2\pi=11.2133$ MHz/T) nuclei using spin-echo technique with a pulse sequence $5\mu\text{s}-\tau_D-10\mu\text{s}$, where the time between pulses τ_D was $40\mu\text{s}$. The spectra were collected by sweeping the applied magnetic field within $8 < H < 93$ kOe at constant frequencies. Low temperatures $0.6 < T < 3.3$ K were achieved with a ${}^3\text{He}/{}^4\text{He}$ dilution refrigerator of Oxford Instruments. The temperatures were stabilized with a precision better than 0.02 K.

III. MAGNETIC SUSCEPTIBILITY

Figure 4 displays the temperature dependence of the molar susceptibility $\chi(T)$ of LiCuVO_4 with the applied magnetic field H directed along the principal axes of the single crystal. The molar susceptibility $\chi(T)$ exhibits two characteristic maxima: the high-temperature maximum around $T \approx 28$ K is usual for low-dimensional magnetic systems and it is associated with the appearance of magnetic correlations within the copper chains. The sharp

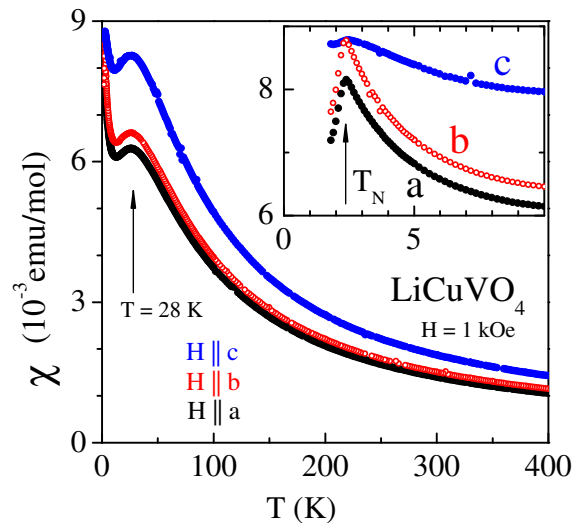


FIG. 4: Temperature dependences of the molar susceptibility $\chi(T)$ of LiCuVO_4 . The applied magnetic field of $H = 1$ kOe was directed along the principal axes **a**, **b** and **c** of the single crystal. Inset: Magnification of the low-temperature range for $T < 10$ K.

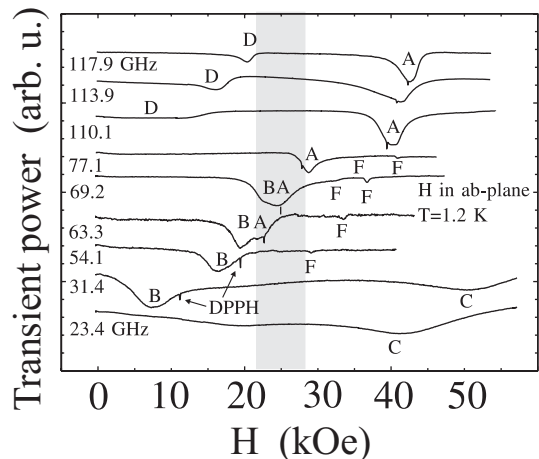


FIG. 5: Transient microwave power vs. applied magnetic field H ($H \parallel \text{ab-plane}$ at 1.2 K). The signal of the reference compound diphenyl-picryl-hydrazyl (DPPH) is marked. For the denotations with capital letters A, ..., F see text.

low-temperature maximum (cf. the inset of Fig. 4) is associated with the transition into a 3D magnetically ordered phase at $T_N = 2.3$ K (Refs. 10,11). The behavior of $\chi(T)$ with respect to $H \parallel \text{a}$ and $H \parallel \text{b}$ is almost the same, but it essentially differs from $\chi(T)$ for $H \parallel \text{c}$. In the paramagnetic phase and in the 3D ordered phase, the values of $\chi(T)$ for $H \parallel \text{c}$ are remarkably enhanced compared to $\chi(T)$ for H lying in the **ab**-plane due to the anisotropy of the g -tensor¹¹.

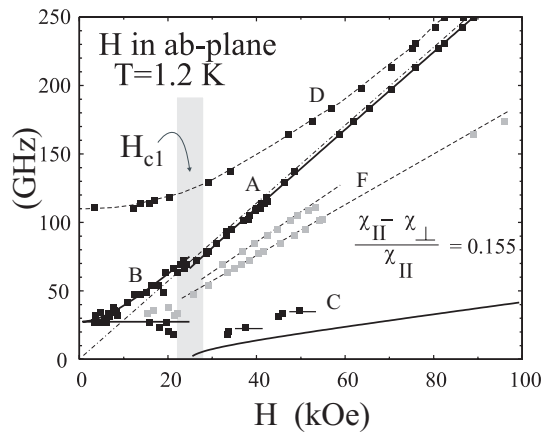


FIG. 6: AFMR spectra in the 3D ordered phase vs. applied magnetic field H ($\mathbf{H} \parallel \mathbf{ab}$ -plane at 1.2 K). The capital letters mark the different branches of the spectra according to the denotations in Fig. 5.

IV. AFMR

In Fig. 5 we show examples of traces of the transient microwave power which are obtained by sweeping the applied magnetic field H . The orientation of \mathbf{H} was chosen to lie within the \mathbf{ab} -plane. All traces were recorded at the temperature $T = 1.2$ K, which is nearly two times less than T_N . The capital letters 'A', ..., and 'F' denote absorption lines. Four absorption lines 'A, B, C, D' revealed intense signals, whereas the absorption line 'F' is characterized by a narrow width and a tiny intensity. It turned out that the rotation of the applied magnetic field \mathbf{H} within the $\mathbf{a, b}$ -plane does not change the position of the absorption lines. The resonance positions of these absorption lines 'A', ..., and 'F' are plotted in Fig. 6 as a function of the magnetic field H . The resonance positions of the narrow line with small intensity, which is marked with the letter 'F' (the grey squares in Fig. 6), most probably have to be attributed to an electron paramagnetic resonance (EPR) of impurities in the sample. This assumption is corroborated by the observation of an decreasing intensity towards higher temperatures, but temperature independent resonance positions of these lines 'F'. Therefore, the absorption lines 'F' will not be discussed in our paper.

Within the field region $22 \lesssim H \lesssim 28$ kOe, which is marked in light grey in Figs. 5 and 6, a peculiarity in the AFMR spectra was observed: towards lower fields H , the branch 'A' transforms into the branch 'B' exhibiting a coexistence of both absorption lines. The absorption line 'A' appears at slightly higher fields, and the absorption line 'B' at slightly lower fields with respect to the resonance of the reference compound diphenyl-picryl-hydrazyl (DPPH, $g = 2$), respectively (cf. Fig. 5). This peculiarity for applied magnetic fields around 25 kOe we associate with a phase transition, most probably of the spin-flop type at $H_{c1} \approx 25$ kOe. For the orientation

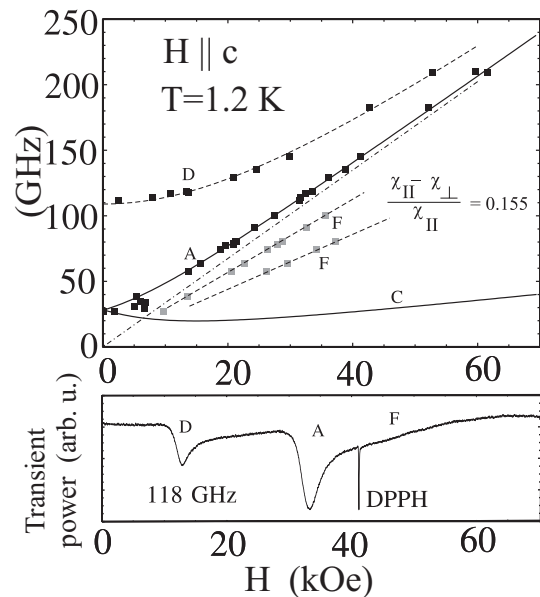


FIG. 7: Upper panel: AFMR spectra in the 3D ordered phase vs. applied magnetic field H ($\mathbf{H} \parallel \mathbf{c}$ at 1.2 K). The capital letters 'A, D, F' mark different branches of the spectra (see text). Lower panel: one example of the trace of the transient microwave power vs. applied magnetic field H at 118 GHz ($\mathbf{H} \parallel \mathbf{c}$ at 1.2 K). The signal of the reference compound DPPH is marked.

of the applied magnetic field $\mathbf{H} \parallel \mathbf{c}$, two branches 'A' and 'D' of the AFMR spectra were observed as shown in figure 7. The dashed-dotted lines in Figs. 6 and 7 show the branches of EPR spectra, which were measured at 4.2 K. The values of the g -factors at 4.2 K are in a good agreement with the values reported in reference 11. The solid lines in Figs. 6 and 7 show the AFMR spectra which were deduced from a phenomenological theory for model systems as explained later in the section VII. The dashed lines in Figs. 6 and 7 are drawn for simplicity of perception.

Figure 8 shows the dependence of the resonance field of the 'A'-branch on the angle ϕ at the temperature of 1.2 K, where ϕ is the angle between the direction of the applied magnetic field \mathbf{H} and the \mathbf{c} -axis. The field \mathbf{H} is applied within the \mathbf{ac} -plane. The open squares mark values of EPR fields, measured in the paramagnetic phase at $T = 4.2$ K for $\mathbf{H} \parallel \mathbf{a}$ and $\mathbf{H} \parallel \mathbf{c}$, respectively. At 78.5 GHz (upper panel), the resonance field for the 'A'-branch occurs at a field value which is smaller than the field of the EPR signal, when the field \mathbf{H} is applied along the \mathbf{c} -axis ($\mathbf{H} \parallel \mathbf{c}$). In case of the orientation $\mathbf{H} \parallel \mathbf{a}$, the resonance field for the 'A'-branch slightly exceeds the field of the EPR signal. The lower panel of Fig. 8 displays the situation at a frequency of 37.7 GHz. Here, the resonances according to this frequency take place at fields less than the transition field $H_{c1} \approx 25$ kOe. In this case, the resonance fields for all angles ϕ are less than the EPR fields. Note that the angular dependences of the resonance fields predominantly are defined by the

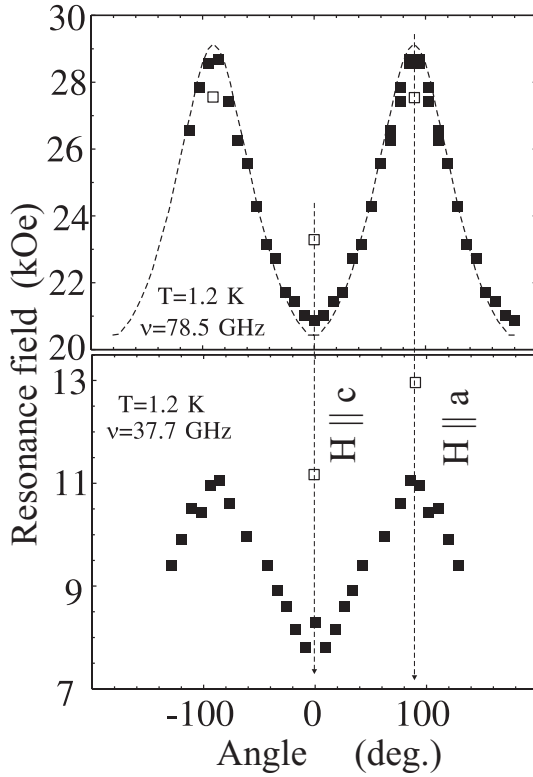


FIG. 8: Resonance field of the 'A' branch vs. $\phi = \angle(\mathbf{H}, \mathbf{c})$ at $T = 1.2$ K. The field \mathbf{H} is applied within the \mathbf{ac} -plane. The open squares mark values of EPR fields, measured in the paramagnetic phase ($T = 4.2$ K) for $\mathbf{H} \parallel \mathbf{a}$ and $\mathbf{H} \parallel \mathbf{c}$, respectively. Upper panel: $\nu = 78.5$ GHz; lower panel: $\nu = 37.7$ GHz.

angular dependence of the g -factor.

On closer inspection of the experimental AFMR data in Figs. 6 and 7 for applied fields $H \rightarrow 0$, there are two branches which exhibit an frequency-axis intercept of $\nu(H = 0) \approx 25$ GHz and ≈ 108 GHz, respectively. These two intercepts at 1.2 K deep in the 3D magnetically ordered phase identify two excitation gaps which turned out to have different temperature dependences: the low-frequency gap decreases with increasing temperatures, and the according branch becomes gapless at a temperature near T_N . In Fig. 9, traces of the transient microwave power are displayed as a function of the applied magnetic field H for different temperatures at $\nu = 24$ GHz. Towards decreasing temperatures, the AFMR line starts to broaden at a temperature $T \approx T_N$ and shifts toward lower fields. At 1.2 K, the broad line at zero field $H = 0$ shows that the probing frequency of 24 GHz is almost equal to the gap value at this temperature. Using equation 2, analogous spectra obtained at the probing frequency of $\nu = 38$ GHz allow to obtain the temperature dependence of the gap value, which is shown in the lower panel of figure 10. The high-frequency gap, which has to be attributed to the 'D'-branch, remains to be open till much higher temperatures than T_N . The upper panel of Fig. 10 shows traces of the

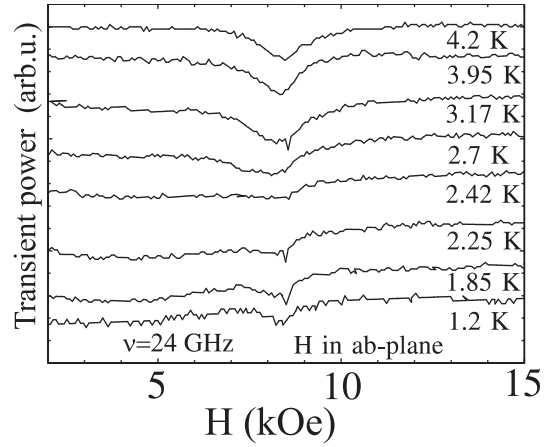


FIG. 9: Transient microwave power vs. applied magnetic field H for different temperatures at 24 GHz. The field \mathbf{H} is applied within the \mathbf{ab} -plane.

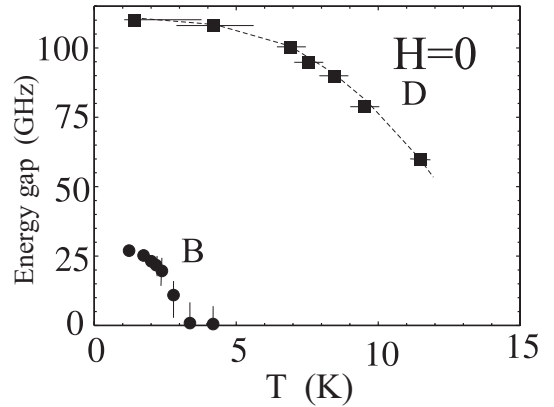
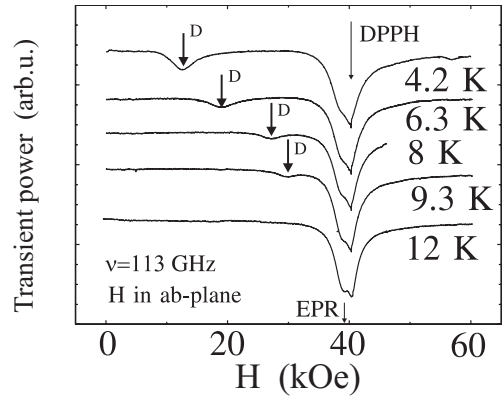


FIG. 10: Upper panel: transient microwave power vs. applied magnetic field H for different temperatures at 113 GHz ($\mathbf{H} \parallel \mathbf{a}$). Lower panel: temperature dependence of the AFMR positions of 'B' and 'D' branches at zero field $H = 0$.

transient microwave power as a function of the applied magnetic field H for different temperatures at $\nu = 113$ GHz ($\mathbf{H} \parallel \mathbf{a}$). The AFMR position of the 'D'-branch is well defined till $T \approx 10$ K. The temperature dependence of this shift of the AFMR position is documented in the lower panel of figure 10. The continuous decrease of the

AFMR frequency towards higher temperatures indicates the closing of the gap. From the extrapolation of this continuous decrease to zero frequency we expect the 'D' branch to be gapless at the temperature of $T \simeq 13$ K.

V. NMR

Figures 11 and 12 show ${}^7\text{Li}$ NMR spectra for different temperatures obtained at the frequencies of $\nu = 22$ MHz and 50 MHz, respectively. The magnetic field H was applied along all crystallographic axes ($\mathbf{H} \parallel \mathbf{a}$, $\mathbf{H} \parallel \mathbf{b}$, and $\mathbf{H} \parallel \mathbf{c}$). These frequencies correspond to applied magnetic fields H which are lower than $H_{c1} \approx 25$ kOe in the case of 22 MHz, and higher than H_{c1} in the case of 50 MHz. For temperatures within the paramagnetic phase ($T \geq 3$ K), the spectra for both frequencies are almost unshifted with respect to the reference field $H_{\text{ref}} = \nu/\gamma$ which is indicated by an arrow in figures 11 and 12. For decreasing temperatures towards T_N , the spectra start to broaden. For temperatures lower than T_N , the spectra change to a plateau-like shape with some increase of the intensity at their borders. Such shape of NMR spectra is characteristic for a spiral structure of the ordered electron moments, in which the magnetic ions induce different effective magnetic fields at the probing NMR nuclei, where the nuclei occupy crystallographically equivalent sites. From the fact of the temperature independent NMR line shape for temperatures $0.6 < T < 1.2$ K we conclude that the AFMR experiments at 1.2 K were performed with nearly saturated magnetic Cu^{2+} moments.

At 22 MHz for applied fields $H < H_{c1}$ (Fig. 11), the NMR spectrum at 0.6 K by application of the magnetic field along \mathbf{c} was approximately three times broader than the spectra observed by orientation of the field along \mathbf{a} and \mathbf{b} . We also measured at the frequency of 14.5 MHz (corresponding to an applied magnetic field around 8.8 kOe, not shown) and it turned out that the line shape at 0.6 K for $\mathbf{H} \parallel \mathbf{b}$ is not changed compared to the spectrum obtained at 22 MHz (cf. uppermost frame of Fig. 11). At 50 MHz for applied fields exceeding H_{c1} (Fig. 12), the broad characteristic NMR spectra shape was observed for orientations of the magnetic field \mathbf{H} parallel to \mathbf{b} and \mathbf{c} . For the orientation $\mathbf{H} \parallel \mathbf{a}$, the NMR spectrum remains to be about three times narrower.

Figures 13 and 14 give the frequency/field dependence of ${}^7\text{Li}$ NMR spectra in the paramagnetic phase at $T = 3.3$ K and in the 3D magnetically ordered phase at $T = 0.6$ K, respectively. In the paramagnetic phase at $T = 3.3$ K (cf. Fig. 13), we observed one single, unsplit spectral line for all frequencies and field orientations and a minor line shift with respect to the diamagnetic reference field $H_{\text{ref}} = \nu/\gamma$ which is indicated by an arrow in figure 13. For the field orientation $\mathbf{H} \parallel \mathbf{a}$, there is no frequency/field dependence of the ${}^7\text{Li}$ NMR line width, whereas for $\mathbf{H} \parallel \mathbf{b}$ and $\mathbf{H} \parallel \mathbf{c}$ an appreciable increase of

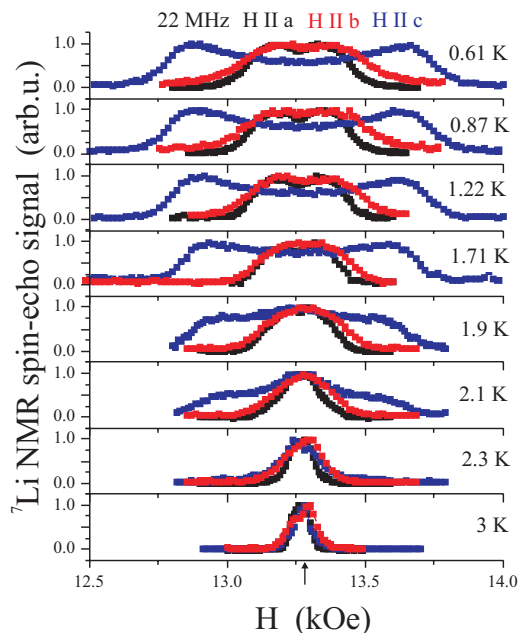


FIG. 11: Temperature dependence of ${}^7\text{Li}$ NMR spectra at 22 MHz. The applied magnetic field \mathbf{H} was oriented along all crystallographic axes \mathbf{a} , \mathbf{b} , and \mathbf{c} .

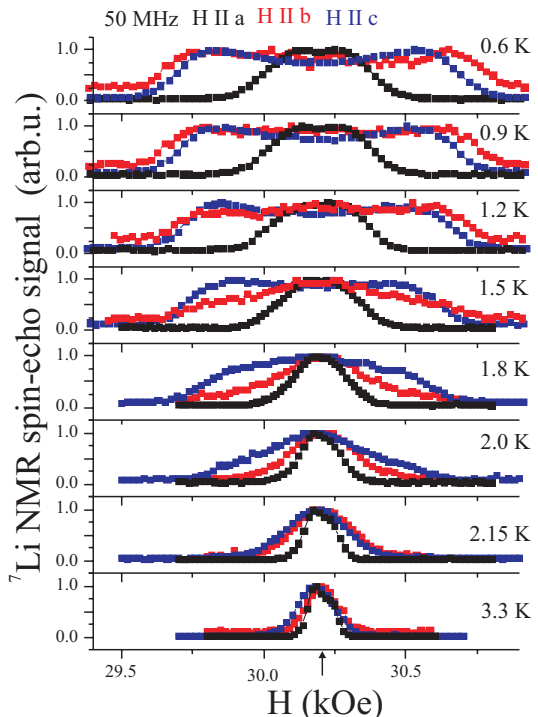


FIG. 12: Temperature dependence of ${}^7\text{Li}$ NMR spectra at 50 MHz. The applied magnetic field \mathbf{H} was oriented along all crystallographic axes \mathbf{a} , \mathbf{b} , and \mathbf{c} .

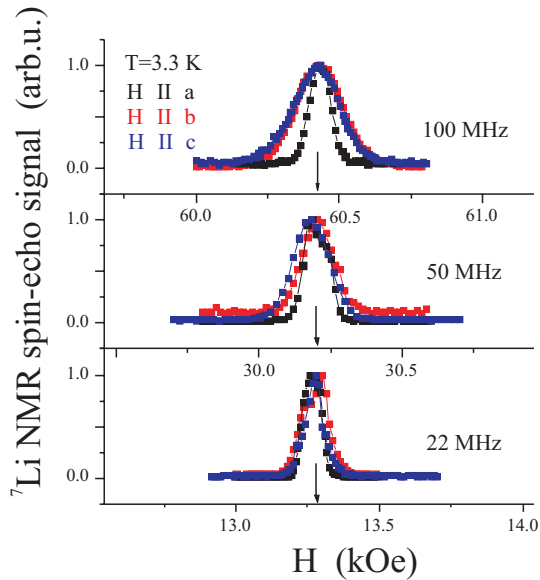


FIG. 13: Frequency dependence of ${}^7\text{Li}$ NMR spectra in the paramagnetic phase at 3.3 K. The applied magnetic field \mathbf{H} was oriented along all crystallographic axes \mathbf{a} , \mathbf{b} , and \mathbf{c} .

the ${}^7\text{Li}$ NMR line width became apparent towards higher frequencies/fields as clearly seen in the uppermost frame of figure 13. In the 3D magnetically ordered phase at $T = 0.6$ K (cf. Fig. 14), the line width of the characteristic spectra shape for $\mathbf{H} \parallel \mathbf{c}$ turned out to be frequency/field independent up to the frequency of 100 MHz and/or field of 60.5 kOe, respectively. However, the line intensity of the central part of these spectra increases with increasing frequency/field. At 100 MHz/60.5 kOe, a plateau-like shape evolved from the double-horn shape at 22 MHz/13.25 kOe. As the frequency/field is further increased to 170 MHz/102.75 kOe, the shape of the ${}^7\text{Li}$ NMR spectra changes to one single, unsplit spectral line (uppermost frame of Fig. 14). As high-field magnetization measurements revealed a spin reorientation taking place at an applied magnetic field of $H_{c2} \approx 75$ kOe (Ref. 12), we interpolate for the change to one single, unsplit spectral line to take place at $H_{c2} \approx 75$ kOe.

Figure 15 shows the orientation dependence of ${}^{51}\text{V}$ NMR spectra in the 3D magnetically ordered phase at 0.6 K for $\nu = 100$ MHz. The intense narrow lines at around 88.4 kOe are due to the ${}^{63}\text{Cu}$ NMR signal from the copper wire of the resonant circuit. For all three crystallographic axes \mathbf{a} , \mathbf{b} , and \mathbf{c} , the line splitting of the ${}^{51}\text{V}$ NMR spectra amounts to five times the splitting of the ${}^7\text{Li}$ NMR spectra. The characteristic NMR line shape of ${}^{51}\text{V}$ for $\mathbf{H} \parallel \mathbf{c}$ has also been observed in a recent NMR study at 120 kOe (Ref. 13). Due to a much stronger hyperfine coupling of the ${}^{51}\text{V}$ nuclei,¹⁰ the effective magnetic fields induced by the Cu^{2+} moments are strongly enhanced compared to the effective local fields induced at the ${}^7\text{Li}$ nuclei. We also tried to detect ${}^{51}\text{V}$ NMR spin-echo signals in the low-field range for $H < H_{c1}$, but for all three crystallographic axes \mathbf{a} , \mathbf{b} , and \mathbf{c} our attempts

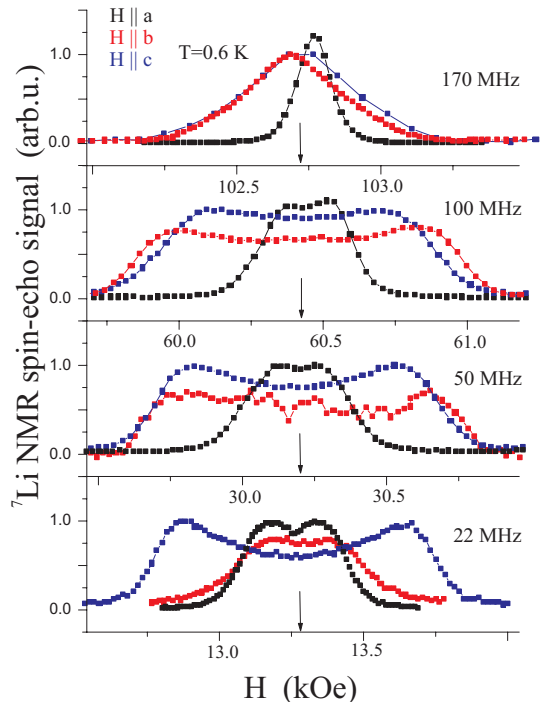


FIG. 14: Frequency dependence of ${}^7\text{Li}$ NMR spectra in the 3D magnetically ordered phase at 0.6 K. The applied magnetic field \mathbf{H} was oriented along all crystallographic axes \mathbf{a} , \mathbf{b} , and \mathbf{c} .

were unsuccessful. We attribute the lack of a vanadium signal to very short spin-spin relaxation times in this field range.

VI. DISCUSSION OF NMR EXPERIMENTS

The magnetic structure of LiCuVO_4 is defined by strongly bonded chains of magnetic Cu^{2+} ions, directed along the crystallographic \mathbf{b} -axis. The intra- and interchain exchange integrals are defined in Ref. 3: the intrachain exchange integrals J_1 and J_2 between nearest and next-nearest moments of copper ions in the chain are -1.6 and 5.6 meV, respectively (cf. Fig. 1). The interchain exchange integrals J_3 , J_4 , J_5 , and J_6 between chains given in Fig. 2 amount to 0.01, -0.37, -0.014 and 0.08 meV, respectively.

The interchain interactions between the chains along the direction of the \mathbf{a} -axis are defined by the exchange integrals J_3 and J_4 yielding a co-ordered arrangement of magnetic moments of neighboring copper ions in this direction. This interaction is much stronger than the interaction along \mathbf{ac} -diagonal (J_5 , J_6 in Fig. 2), which define the interchain interaction of magnetic moments in neighboring \mathbf{ab} -planes. The simple evaluation of the exchange interactions with these values of exchange integrals give the following hierarchy of energy of interactions recomputed on one magnetic ion: the ferromagnetic interaction between the chains within \mathbf{ab} -planes is about one order

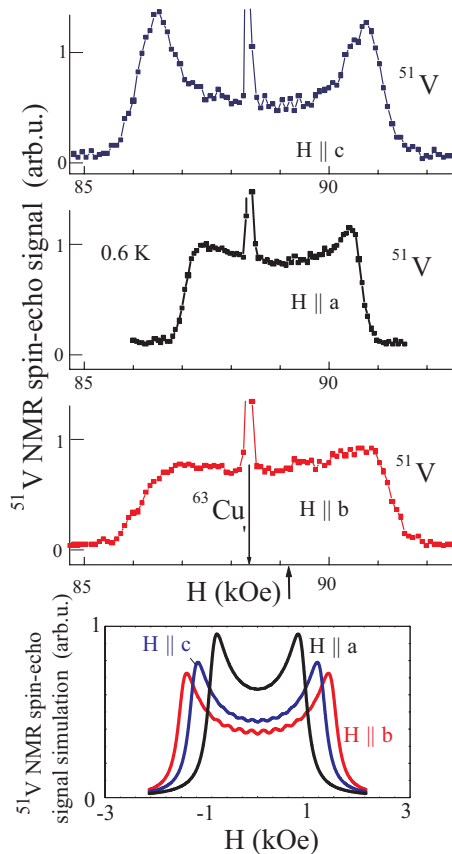


FIG. 15: Upper panel: orientation dependence of ^{51}V NMR spectra in the 3D magnetically ordered phase at 0.6 K and 100 MHz. The applied magnetic field \mathbf{H} was oriented along all crystallographic axes \mathbf{a} , \mathbf{b} , and \mathbf{c} . Lower panel: computed NMR spectra.

of magnitude less than the intrachain interactions and around ten times larger than the antiferromagnetic interaction between neighboring \mathbf{ab} -planes. The magnetic moments of Cu^{2+} ions in neighboring \mathbf{ab} -planes are oriented antiparallel.²

In the present paper we study NMR on ^7Li and ^{51}V nuclei. In Fig. 2, the positions of one Li^+ ion and one V^{5+} ion are shown exemplarily, and it turns out that the lattice positions of these ions are essentially different: the position of the Li^+ ions contains the operation of inversion, but the position of V^{5+} does not. The ^7Li nuclei reside on positions between neighboring \mathbf{ab} -planes. Every lithium ion has four nearest copper ions, which are equally distanced from it. Each vanadium ion resides between six neighboring copper ions, at that, four of them belong to one \mathbf{ab} -plane, and two, more distant, to another \mathbf{ab} -plane.

The effective local fields at the probing nuclei of the nonmagnetic lithium and vanadium ions are composed of the long-range dipole fields of surrounding magnetic moments and of the so called "contact" hyperfine fields due to the nearest magnetic ions. The contact fields are ex-

pected to be proportional to the spin values of the neighboring copper ions. The contact fields at the ^7Li nuclei must be self-compensated in the case of the antiparallel magnetic ordering of the nearest magnetic moments of neighboring \mathbf{ab} -planes. At the ^{51}V nuclei, the contact fields will be predominantly given by the spins of the four nearest magnetic ions of the nearest neighboring \mathbf{ab} -plane (cf. Fig. 2). The value of the long-range dipole field was computed for the positions of ^7Li and ^{51}V nuclei by assumption of the spiral magnetic structure proposed in reference 2. For this structure, the magnetic moments of the copper ions can be calculated:

$$\mu = \mu_{\text{ord}} \cdot \mathbf{l}_1 (-1)^{2z/c} \cdot \cos(k_{ic} \cdot y) + \mu_{\text{ord}} \cdot \mathbf{l}_2 (-1)^{2z/c} \cdot \sin(k_{ic} \cdot y), \quad (1)$$

where the coordinates x, y , and z are given in the basis of the crystal axes \mathbf{a}, \mathbf{b} , and \mathbf{c} . The vectors \mathbf{l}_1 and \mathbf{l}_2 are orthogonal unit vectors within the \mathbf{ab} -plane. Consequently, the vector of the exchange structure $\mathbf{n} = \mathbf{l}_1 \times \mathbf{l}_2$ is parallel to the \mathbf{c} -axis. The values of the lattice parameters a, b and c , and the coordinates of lithium and vanadium ions were taken from reference 14. For the value of the ordered magnetic moment μ_{ord} of copper ions we took $0.31 \mu_B$ as it was obtained in reference 2.

$H < H_{c1}$:

The dipole field at the ^7Li nuclei depends on their positions within the incommensurate spiral magnetic structure. In the upper panel of Fig. 16, the projections of dipole fields on the \mathbf{a} -, \mathbf{b} -, and \mathbf{c} -axes are plotted as a function of the phase of the spiral magnetic structure. From these fields it is simple to simulate the expected NMR spectra for all three directions of the applied magnetic field H with respect to the crystallographic axes. The lower panel of Fig. 16 shows computed spectra (solid lines) and experimental data (symbols) for the frequency of 22 MHz. This computation was performed with a Lorentzian shape of the NMR spectrum which is produced by the group of ^7Li nuclei experiencing the same value of the effective local magnetic field. The line width of this Lorentzian-shaped spectrum was assumed to be equal to 75 Oe. This value of the line width is consistent with the line width in the paramagnetic phase of the low-field range (Fig. 11). The computed NMR spectra are in a very good agreement with the experimental spectra. That means that the effective local fields at the ^7Li nuclei are predominantly defined by long-range dipole fields, and we should be able to specify the magnetic structures of LiCuVO_4 for elevated applied magnetic fields $H > H_{c1}$.

$H_{c1} < H < H_{c2}$:

The most natural magnetic transition taking place with increasing applied magnetic fields H is the spin-flip transition, i.e. the rotation of the plane of the spiral spin structure perpendicular to the direction of the applied magnetic field H . Therefore, for $\mathbf{H} \parallel \mathbf{c}$ there will be no spin reorientation expected. Indeed, the

experiment exhibits nearly the same pattern of the NMR spectra for $\mathbf{H} \parallel \mathbf{c}$ at all frequencies 22 MHz, 50 MHz, and 100 MHz, corresponding to applied magnetic fields around $H_{c1} \approx 25$ kOe (cf. Fig. 14). Applying a magnetic field $H > H_{c1}$ parallel to the \mathbf{a} - and \mathbf{b} -axes may result in a rotation of the magnetic structure and the line shapes concomitantly can change. Figure 17 shows the results of the computation of the NMR spectra for these structures together with the experimental NMR spectra measured at the frequency of 50 MHz. The computation and experiment show that the spin reorientation drastically broadens the NMR spectra for $\mathbf{H} \parallel \mathbf{b}$, and nearly no change is observed for $\mathbf{H} \parallel \mathbf{a}$. This magnetic structure is maintained up to applied magnetic fields $H \approx 60.5$ kOe $< H_{c2}$, as it is seen from the NMR spectra pattern at 100 MHz/60.5 kOe in figure 14. Thus for $H_{c1} < H < H_{c2}$, the magnetic structure exhibits the spiral plane to be perpendicular to the applied magnetic field $\mathbf{H} \parallel \mathbf{n}$ (cf. Eq. 1) for $\mathbf{H} \parallel \mathbf{b}$ and $\mathbf{H} \parallel \mathbf{c}$, respectively. The agreement of the experimental and computed spectra only was possible to obtain in the case of an antiferromagnetic alternation of the magnetic moments of neighboring \mathbf{ab} -planes (cf. Fig. 2).

$H > H_{c2}$:

A more complicate situation occurs at high fields $H > H_{c2}$: the NMR spectra of ${}^7\text{Li}$ nuclei in this field range consist of one single line for all field directions (cf. the uppermost panel in Fig. 14), indicating a second spin reorientation process to take place. For the high field range $H > H_{c2}$ it was possible to measure NMR spectra of the ${}^{51}\text{V}$ nuclei, too. To understand the nature of the effective local field at the ${}^{51}\text{V}$ nuclei we computed the long-range dipole field at the vanadium site for the paramagnetic phase. The computed dipole field is -0.44 kOe/ μ_B for the direction of the applied field \mathbf{H} parallel to the \mathbf{b} -axis. But the value of the hyperfine coupling constant ${}^{51}\text{A}_{\parallel\mathbf{b}}=4.95$ kOe/ μ_B is about ten times larger as we obtained in reference 10. Thus we can conclude that the main part of the effective local field at the ${}^{51}\text{V}$ nuclei is defined by contact fields. The value of the effective contact field induced by copper ions at vanadium nuclei can be evaluated as $5.4(\overline{\mu_1}+\overline{\mu_2}+\overline{\mu_3}+\overline{\mu_4})/4$ kOe/ μ_B . Here we take into account only the four nearest magnetic copper ions from the nearest neighboring \mathbf{ab} -plane (Fig. 2).

The characteristic broad NMR spectra of ${}^{51}\text{V}$ nuclei (Fig. 15) in the 3D magnetically ordered phase for $H > H_{c2}$ indicate a modulation of the projection of the Cu^{2+} moments on the direction of the applied field \mathbf{H} . A more simple way to describe these modulation is to suppose that at H_{c2} the spiral planar magnetic structure orients to be parallel to the applied field H (i.e., $\mathbf{n} \perp \mathbf{H}$). We computed the value of the effective local fields at the ${}^{51}\text{V}$ nuclei using the same parameters k_{ic} and μ_{ord} of the spiral magnetic structure at zero applied field $H=0$. The computed NMR spectra with these parameters are shown in the lowest panel of figure 15. Again, this computation was performed with a Lorentzian shape of the

NMR spectrum which is produced by the group of ${}^{51}\text{V}$ nuclei experiencing the same value of the effective local magnetic field. The line width of this Lorentzian-shaped spectrum was assumed to be equal to 150 Oe. Note that the computed NMR spectra better fit, if the value of μ_{ord} is increased and/or the value of k_{ic} is decreased.

Changing again to the ${}^7\text{Li}$ NMR spectra for $H > H_{c2}$ (cf. upper panel in Fig. 18), the unsplit line shapes of the NMR spectra suggest the following magnetic structures which are deduced from computations of dipole fields for different planar spiral structures: for $\mathbf{H} \parallel \mathbf{c}$, the best fit is obtained for $\mathbf{n} \parallel \mathbf{b}$. For $\mathbf{H} \parallel (\mathbf{a}, \mathbf{b})$, the plane of the spiral structure lies within the \mathbf{ab} -plane (i.e., $\mathbf{n} \parallel \mathbf{c}$). In the lower panel of Fig. 18 the results of the computed NMR spectra are shown for these spiral structures. For field orientations parallel to the \mathbf{a} - and \mathbf{b} -axes, the computed spectra exhibit some splitting of the spectra shape contrary to the experiment. Due to this lack of any splitting of the experimental spectra for $H > H_{c2}$ we conclude that *not* the spiral-, but a spin-modulated structure is realized, i.e. the spin projections perpendicular to the direction of the applied field H are disordered. The NMR spectra computed for this spin-modulated structure are shown in the same figure (dashed lines in the lower panel of Fig. 18). All spectra for this structure are unsplit. This computation was performed with a line width of 150 Oe of the Lorentzian-shaped NMR spectrum which is produced by the group of ${}^7\text{Li}$ nuclei experiencing the same value of the effective local magnetic field. In order to achieve a better fit for field directions $\mathbf{H} \parallel (\mathbf{b}, \mathbf{c})$, this value of the line width has to be increased by a factor of 2.8. At first glance this increase seems to be arbitrary, but on closer inspection of the experimental spectra in the paramagnetic phase (uppermost panel of Fig. 13), the spectral line widths for field directions $\mathbf{H} \parallel (\mathbf{b}, \mathbf{c})$ are also significantly increased compared to $\mathbf{H} \parallel \mathbf{a}$.

VII. DISCUSSION OF AFMR EXPERIMENTS

For low applied magnetic fields $H < H_{c1}$, the authors of Ref. 2 propose the planar spiral structure for the magnetic structure of LiCuVO_4 in the 3D magnetically ordered phase. This structure was found to be defined by strong exchange interactions within the magnetic chains.³ Our results of the NMR and susceptibility χ investigations can be explained on the same footing. The results of EPR (Ref. 11) and AFMR (this work) hint towards an uniaxial character of the crystal anisotropy in LiCuVO_4 . These observations motivate to discuss the low-field AFMR data in the assumptions of an exchange-rigid planar uniaxial magnetic structure with an uniaxial crystal anisotropy, which is directed along the \mathbf{c} -axis. Thus, we will suppose that the susceptibility of the exchange structure will be defined by two values χ_{\parallel} and χ_{\perp} , i.e. along and perpendicular to the vector of the exchange structure \mathbf{n} (cf. Eq. 1), respectively. The anisotropy energy within this model can be written in a

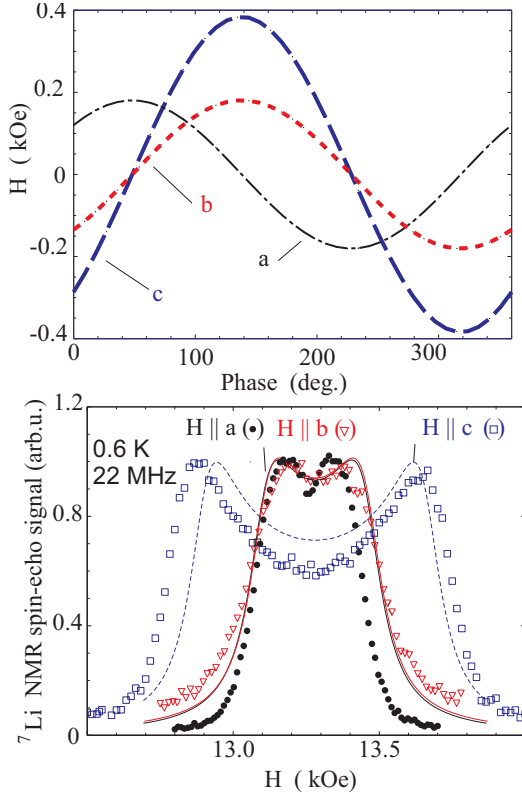


FIG. 16: Upper panel: computed projections of dipole fields along the **a**, **b**, and **c** axes as a function of the phase of the spiral magnetic structure $\mathbf{n} \parallel \mathbf{c}$ suggested in Ref. 2. Lower panel: experimental ${}^7\text{Li}$ NMR spectra measured at $T = 0.6$ K for $H < H_{c1}$ (symbols) and computed NMR spectra (dashed and solid lines).

form $\beta n_z^2/2$ ($\beta < 0$). The NMR and AFMR data reveal a magnetic transition at H_{c1} , if the magnetic field H is applied parallel to the **ab**-plane. This implies that χ_{\parallel} is larger than χ_{\perp} , and the transition field can be described as $H_{c1}^2 = \beta/(\chi_{\perp} - \chi_{\parallel})$.

In Ref. 15, the low-frequency branches of the AFMR spectra for noncollinear coplanar structures with an uniaxial anisotropy were obtained in the framework of a phenomenological theory according to reference 16. The spectra of acoustic modes consist of three branches, which correspond to three rotational degrees of freedom. In the case of an uniaxial exchange structure, one branch out of these three branches must be zero ($\nu=0$), which is attributed to the rotational degree of freedom of the exchange structure around the **n**-axis. The frequencies of the two other branches can be obtained from the square equation:

$$(\nu/\gamma)^4 - (\nu/\gamma)^2 \{ H^2 + \eta^2 H^2 \cos^2(\theta - \phi) + \eta H_{c1}^2 (3 \cos^2 \theta - 1) \} + \eta \{ -H_{c1}^2 \cos^2 \theta - H^2 \cos^2(\theta - \phi) \} \{ -\eta H_{c1}^2 \cos 2\theta - \eta H^2 \cos^2(\theta - \phi) - H^2 \sin^2(\theta - \phi) \} = 0, \quad (2)$$

where $\gamma = g\mu_B/2\pi\hbar$, $\eta = (\chi_{\parallel} - \chi_{\perp})/\chi_{\perp}$ and $\phi = \angle(\mathbf{H}, \mathbf{c})$ is

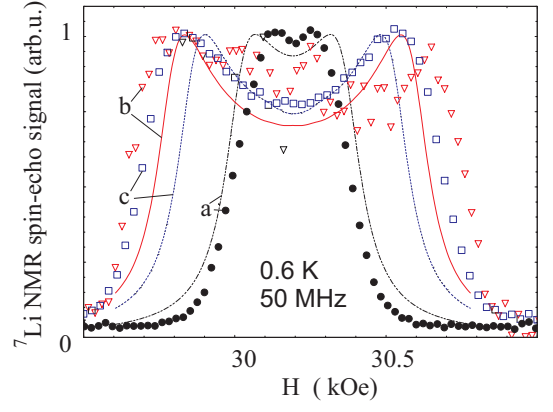


FIG. 17: Experimental ${}^7\text{Li}$ NMR spectra measured at $T = 0.6$ K and $H > H_{c1}$ (symbols) and computed NMR spectra (dashed and solid lines).

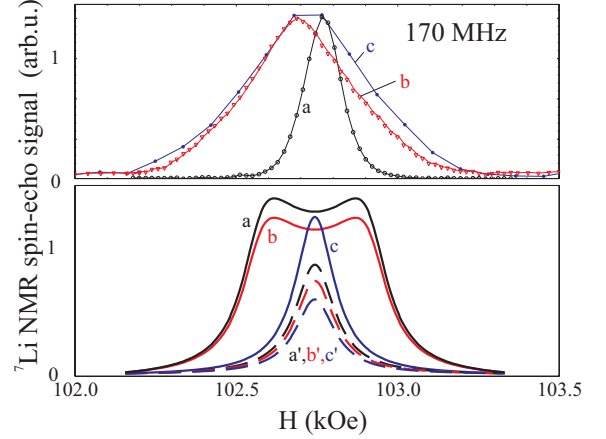


FIG. 18: Upper panel: experimental ${}^7\text{Li}$ NMR spectra measured at $T = 0.6$ K and $H > H_{c2}$. The applied magnetic field \mathbf{H} was oriented along all crystallographic axes **a**, **b**, and **c**. Lower panel: computed NMR spectra for spiral- (solid lines, **a**, **b**, and **c**) and spin-modulated structure (dashed lines, **a'**, **b'**, and **c'**), respectively.

the angle between the crystallographic **c**-axis and the direction of the applied magnetic field \mathbf{H} . The angle $\theta = \angle(\mathbf{n}, \mathbf{c})$ is defined by:

$$\tan(2\theta) = \frac{H^2 \sin 2\phi}{H^2 \cos(2\phi) + H_{c1}^2}$$

If the applied magnetic field is directed along the **c**-axis ($\mathbf{H} \parallel \mathbf{c}$), both angles are zero ($\theta=0$, $\phi=0$). Whereas,

$$\begin{aligned} \text{for } \mathbf{H} \perp \mathbf{c}, H < H_{c1} : \theta = 0, \phi = \pi/2, \\ \text{for } \mathbf{H} \perp \mathbf{c}, H > H_{c1} : \theta = \pi/2, \phi = \pi/2. \end{aligned}$$

At zero applied field $H=0$, the frequency of both oscillations must be $\nu_{1,2} = \gamma H_{c1} \sqrt{\eta}$. Taking the frequency of 27 ± 2 GHz of the AFMR at zero applied field and the field H_{c1} of the spin-flop transition to be $H_{c1} = 25 \pm 3$ kOe,

we obtain the parameter of the anisotropy of the exchange susceptibility $\eta=0.155\pm 0.05$, and the value of the anisotropy constant $\beta = -0.01$ K, recomputed on one copper ion. The results of the computation of the 'A', 'B', and 'C' branches of the AFMR spectra for $\eta=0.155$ are shown as solid lines in Figs. 6 and 7. The value of the anisotropy of the exchange parameter η is in satisfactory agreement with the value obtained from susceptibility measurements at low fields (Fig.4). Note, the theory of AFMR spectra discussed above is developed in an exchange approximation with isotropic γ . For the computed spectra shown in Figs. 6 and 7 we used the values of $\gamma_{\parallel} = 3.25$ GHz/kOe and $\gamma_{\perp} = 2.85$ GHz/kOe, which were measured in the paramagnetic phase. We can conclude that this model describes the AFMR spectra within the low-field range ($H \ll H_{c2}$) very well.

The magnetic phase H - T diagram of LiCuVO_4 is rich not only in field cut, but in temperature also. It seems that the establishment of the 3D magnetic order appears through some intermediate phase transition. This we conclude from the fact that the AFMR branch 'D' in Figs. 6 and 7 starts to be gapped at a temperature much higher than T_N ($\simeq 13$ K) (Fig. 10). The fingerprint of this transition around $T = 13$ K additionally has recently been detected in measurements of the temperature dependence of the heat capacity,¹⁷ where a peak of $C(T)$ centered at $T = 12$ K has been reported.

VIII. CONCLUSION

The NMR and AFMR results can be self-consistently described by the following phase diagram:

$$\begin{aligned} H < H_{c1} : \mathbf{n} \parallel \mathbf{c} \\ H_{c1} < H < H_{c2} : \mathbf{n} \parallel \mathbf{H} \\ H_{c2} < H : \mathbf{l}_1 \parallel \mathbf{H} \text{ and } \mathbf{l}_2 = 0, \end{aligned}$$

where the magnetic structures are described in terms of equation 1. It is important to note that for $H > H_{c2}$ from our experiments we can conclude surely only about the presence of a modulation of projections of copper mo-

ments along the direction of the applied magnetic field H with an amplitude of $\approx 0.4\pm 0.1 \mu_B$. The best fit of ^7Li NMR spectra is obtained based on a spin-modulated structure, i.e. the spin components of Cu^{2+} perpendicular to the direction of the applied magnetic field H are disordered.

The low-field phases for $H < H_{c2}$ observed in LiCuVO_4 are natural from the point of view of mean-field theory. The susceptibility of the exchange structure in the direction perpendicular to the \mathbf{a} , \mathbf{b} -plane is larger than the susceptibility within this plane. The competition of the Zeeman energy and the energy of the crystal-field anisotropy explains the low-field transition observed at H_{c1} . The second transition at the field of H_{c2} is unusual. To explain this transition we have to assume that with an increase of the applied magnetic field that structure starts to be preferable which exhibits the spin modulation parallel to the direction of the applied magnetic field, rather than the structure with the spin plane being perpendicular to the field direction. Probably, it is necessary to take into account the thermal and quantum fluctuations in order to explain the situation. For example, for the planar spiral structure on the triangular lattice it was found that some energy gain occurs for the orientation of spin plane to be parallel to the direction of the applied magnetic field.¹⁸

Acknowledgments

We are grateful to A. Pimenova and D. Vieweg for susceptibility measurements. We thank V.N. Glazkov, V.I. Marchenko, A.I. Smirnov, S.S. Sosin, G.B. Teitelbaum, and A. Loidl for useful discussions. This work is supported by the Grants 04-02-17294, 06-02-16509 Russian Foundation for Basic Research, Russian President Program of Scientific Schools, contract BMBF via VDI/EKM 13N6917, and program of the German Research Society within the Sonderforschungsbereich 484 (Augsburg).

* Electronic address: norbert.buettgen@physik.uni-augsburg.de

† present address: Institut für Festkörperphysik Technische Universität Wien, A-1040 Wien, Austria

¹ A.N. Vasil'ev, Pis'ma Zh. Eksp. Teor. Fiz. **69**, 828 (1999) [JETP Letters, **69**, 876 (1999)].

² B.J. Gibson, R.K. Kremer, A.V. Prokofiev, W. Assmus, G.J. McIntyre, Physica **B 350**, 253 (2004).

³ M. Enderle, C. Mukherjee, B. Fåk, R.K. Kremer, J.-M. Broto, H. Rosner, S.-L. Drechsler, J. Richter, J. Malek, A. Prokofiev, W. Assmus, S. Pujol, J.-L. Raggazzoni, H. Rakoto, M. Rheinstädter, and H.M. Rønnow, Europhys. Lett. **70**, 237 (2005).

⁴ Y. Mizuno, T. Tohyama, S. Maekawa, T. Osafune, N. Motoyama, H. Eisaki, and S. Uchida, Phys. Rev. B **57**, 5326

(1997).

⁵ S.R. White and I. Affleck, Phys. Rev. B **54**, 9862 (1996).

⁶ R. Bursill, G.A. Gehring, D.J.J. Farnell J.B. Parkinson, Tao Xiang, and Chen Zeng, J. Phys. Condens. Matter, **7**, 8605 (1995).

⁷ A.V. Prokofiev, D. Wichert, and W. Assmus, J. Cryst. Growth **220**, 345 (2000).

⁸ Ch. Kegler, N. Büttgen, H.-A. Krug von Nidda, A. Krimmel, L. Svistov, B.I. Kochelaev, A. Loidl, A. Prokofiev, and W. Assmus, Eur. Phys. J. B **22**, 321 (2001).

⁹ A.V. Prokofiev, I.G. Vasilyeva, V.N. Ikorskii, V.V. Malakhov, I.P. Asanov and W. Assmus, J. Solid State Chem. **177**, 3131 (2004).

¹⁰ C. Kegler, N. Büttgen, H.-A. Krug von Nidda, A. Loidl, R.

- Nath, A. V. Mahajan, A. V. Prokofiev, and W. Assmus, Phys. Rev. B **73**, 104418 (2006).
- ¹¹ H.-A. Krug von Nidda, L.E. Svistov, M.V. Eremin, R.M. Eremina, A. Loidl, V. Kataev, A. Validov, A. Prokofiev, and W. Assmus, Phys. Rev. B **65**, 134445 (2002).
- ¹² M.G. Banks, F. Heidrich-Meisner, A. Honecker, H. Rakoto, J.-M. Broto, and R.K. Kremer, cond-mat/0608554 v1 (2006).
- ¹³ R. Smith, A.P. Reyes, R. Ashey, T. Caldwell, A. Prokofiev, W. Assmus, and G. Teitelbaum, Physica B **378-380**, 1060 (2006).
- ¹⁴ R. Kanno, Y. Kawamoto, Y. Takeda, M. Hasegawa, O. Yamamoto, and N. Kinomura, J. Solid State Chem. **96**, 397 (1992).
- ¹⁵ I.A. Zaliznyak, V.I. Marchenko, S.V. Petrov, L.A. Prozorova, and A.V. Chubukov, Pis'ma Zh. Eksp. Teor. Fiz. **47**, 172 (1988) [JETP Letters **47**, 211 (1988)].
- ¹⁶ A.F. Andreev and V.I. Marchenko, Usp. Fiz. Nauk **130**, 39 (1980), [Sov. Phys. Usp. **23**, 21 (1980)].
- ¹⁷ M.G. Banks, R.K. Kremer, A. Honecker, and F. Heidrich-Meisner, "Observation of Two Low Temperature Peaks in the Specific Heat and Possible Middle Field Cusp Singularity in the $S = 1/2$ Chain System LiCuVO_4 ", contribution to the conference on Highly Frustrated Magnetism 2006, Osaka, Japan.
- ¹⁸ A.V. Chubukov and D.I. Golosov, J. Phys.: Condens. Matter **3**, 69 (1991).